

Adaptive modulation in the $\text{Ni}_2\text{Mn}_{1.4}\text{In}_{0.6}$ magnetic shape-memory Heusler alloyP. Devi,¹ Sanjay Singh,^{1,2,*} B. Dutta,³ K. Manna,¹ S. W. D'Souza,¹ Y. Ikeda,³ E. Suard,⁴ V. Petricek,⁵ P. Simon,¹ P. Werner,⁶ S. Chadhov,¹ Stuart S. P. Parkin,⁶ C. Felser,¹ and D. Pandey²¹Max Planck Institute for Chemical Physics of Solids, Nöthnitzer Strasse 40, D-01187 Dresden, Germany²School of Materials Science and Technology, Indian Institute of Technology (Banaras Hindu University), Varanasi-221005, India³Max-Planck-Institut für Eisenforschung Max-Planck-Strasse 1, 40237, Düsseldorf, Germany⁴Institut Laue-Langevin, Boîte Postale 156, 38042 Grenoble Cedex 9, France⁵Institute of Physics ASCR, Department of Structure Analysis, Na Slovance 2, 182 21 Praha, Czech Republic⁶Max Planck Institute of Microstructure Physics, 06120 Halle, Germany

(Received 31 October 2016; revised manuscript received 13 May 2018; published 11 June 2018)

The origin of incommensurate structural modulation in Ni-Mn based Heusler-type magnetic shape-memory alloys (MSMAs) is still an unresolved issue in spite of intense focus on it due to its role in the magnetic field induced ultrahigh strains. In the archetypal MSMA Ni_2MnGa , the observation of “nonuniform displacement” of atoms from their mean positions in the modulated martensite phase, premartensite phase, and charge density wave as well as the presence of phason broadening of satellite peaks has been taken in support of the electronic instability model linked with a soft acoustic phonon. We present here results of a combined high-resolution synchrotron x-ray powder diffraction (SXRPD) and neutron powder diffraction (NPD) study on $\text{Ni}_2\text{Mn}_{1.4}\text{In}_{0.6}$ using a (3+1)D superspace group approach, which reveals not only uniform atomic displacements in the modulated structure of the martensite phase with physically acceptable ordered magnetic moments in the antiferromagnetic phase at low temperatures, but also the absence of any premartensite phase and phason broadening of the satellite peaks. Our HRTEM studies and first-principles calculations of the ground state also support uniform atomic displacements predicted by powder diffraction studies. All these observations suggest that the structural modulation in the martensite phase of $\text{Ni}_2\text{Mn}_{1.4}\text{In}_{0.6}$ MSMA can be explained in terms of the adaptive phase model. The present study underlines the importance of superspace group analysis using complementary SXRPD and NPD in understanding the physics of the origin of modulation as well as the magnetic and the modulated ground states of the Heusler-type MSMAs. Our work also highlights the fact that the mechanism responsible for the origin of modulated structure in different Ni-Mn based MSMAs may not be universal and it must be investigated thoroughly in different alloy compositions.

DOI: [10.1103/PhysRevB.97.224102](https://doi.org/10.1103/PhysRevB.97.224102)**I. INTRODUCTION**

Magnetic shape-memory Heusler alloys (MSMAs) in the Ni-Mn- X ($X = \text{Ga}, \text{In}, \text{Sn}$) system have enormous potential for technological applications due to a rich variety of properties ranging from generation of extremely large magnetic field induced strain ($\sim 10\%$) to pronounced magnetocaloric and barocaloric effects, large magnetoresistance, anomalous Hall effect, and large exchange bias [1–6]. The technologically significant physical properties of these alloys are intimately linked with the coupling between structural and magnetic degrees of freedom below the magnetostructural (martensite) phase transition. Since the modulated crystal structure of the martensite phase due to its low detwinning stress is known to play an important role in deciding the response of these alloys to the external magnetic field, there is currently a lot of interest in understanding the origin of the modulated structure of the martensite phase itself [7–17]. Two different models have been proposed in the literature for the origin of modulation in the MSMAs. The first one is the adaptive phase model in which

the modulated structure is considered as a nanotwinned state of the Bain distorted phase, which maintains the invariance of the habit plane between the high-temperature austenite and the low-temperature martensite phases [14, 15]. Commensurate modulated structure, uniform atomic displacements, and the absence of any premartensite phase transition as well as phason strains are the key manifestations of this model. The second model, based on charge density wave (CDW) coupled to a soft transverse acoustic (TA2) mode [18–20], can, on the other hand, explain nonuniform atomic displacements, the incommensurate nature of modulation, and the existence of the premartensite phase as well as phasons [10–12, 21, 22]. It has been proposed that the formation of discommensurations in the form of stacking faults and antiphase boundaries can in principle result in an average incommensurate modulated structure even for the adaptive phase model [14–16]. However, one of the key features for distinguishing between the two models for the origin of modulation is the identification of the nature (uniform versus nonuniform) of the atomic displacements.

Recently we have shown that the origin of modulation in the Ni_2MnGa shape-memory Heusler alloy cannot be explained within the framework of the adaptive phase model as the modulated structure has nonuniform atomic displacements

*sanjay.singh@cpfs.mpg.de

[12]. Also the fact that the incommensurate martensite phase results from an incommensurate premartensite phase and not directly from the austenite phase does not support the adaptive phase model [11]. The presence of phasons [23] and the broadening of the superlattice peaks due to phason strains [12] in Ni_2MnGa also go against the concept of adaptivity. On the other hand, the Ni-Mn-In MSMA do not exhibit the premartensite (precursor) phase formation as the austenite phase transforms directly to the martensite phase. This suggests that these alloys may be model systems for investigating the applicability of the adaptive phase model for structural modulation through a careful analysis of the structure of the martensite phase. Here, we present results of Rietveld analysis of high-resolution synchrotron x-ray powder diffraction (SXRPD) and neutron powder diffraction (NPD) data on a Ni-Mn-In alloy, $\text{Ni}_2\text{Mn}_{1.4}\text{In}_{0.6}$, using the (3+1)D superspace group approach. Our analysis reveals that the modulated structure of the martensite phase of $\text{Ni}_2\text{Mn}_{1.4}\text{In}_{0.6}$ involves uniform displacements of atoms with respect to their positions in the Bain distorted basic cell. This conclusion is well supported by high-resolution transmission electron microscopic studies as well as first-principles calculations of the ground state of these alloys. All these observations comprehensively rule out the applicability of the CDW based soft mode model and support the adaptive modulation model for $\text{Ni}_2\text{Mn}_{1.4}\text{In}_{0.6}$. Further, in contrast to Ni_2MnGa , Rietveld analysis of the neutron powder diffraction pattern reveals antiferromagnetic (AFM) correlations for Mn spins at two different crystallographic positions of the martensite phase with full and partial Mn occupancies. The AFM ordering is further supported by isothermal magnetization measurements that reveal a double hysteresis loop due to a spin-flop transition induced by a very low magnetic field of 0.05 T at 2 K.

II. RESULTS AND DISCUSSION

The details of sample preparation, measurements [magnetization, SXRPD, NPD, and high-resolution transmission electron microscopy (HRTEM)], Rietveld refinements, and first-principles calculations are given in the Supplemental Material [24]; also see [25–36]. The low-field (500 Oe) magnetization curves of $\text{Ni}_2\text{Mn}_{1.4}\text{In}_{0.6}$ recorded under zero field cooled (ZFC), field cooled cooling (FCC) and field cooled warming (FCW) conditions at 0.05 T in the temperature range 2–400 K are shown in Fig. 1(a). It reveals a sharp

jump in magnetization at the Curie temperature $T_c \sim 315$ K due to a ferromagnetic (FM) transition, followed by a decrease in magnetization at the first-order martensite transition temperature $T_M \sim 295$ K. The bifurcation of the ZFC and FCC curves below $T \sim 145$ K is in agreement with earlier reports [3] where it has been attributed to the coexistence of antiferromagnetic and ferromagnetic exchange interactions in the martensite phase [37]. Our isothermal magnetization $M(H)$ plot at 2 K [see Fig. 1(b)] indicates a typical antiferromagnetic ground state with a spin-flop transition occurring at a very low magnetic field of ± 0.05 T leading to the opening up of a double hysteresis loop above this field. The fact that the spin-flop transition occurs at such a low field suggests that both the FM and AFM states are nearly degenerate in the martensite phase, even though the ground state is dominated by AFM interactions.

We now turn towards the structure of the austenite and martensite phases using SXRPD patterns recorded at 350 K (austenite phase) and 235 K (martensite phase), respectively. In the first step of the structure analysis, we performed indexing of the powder diffraction patterns by the Le Bail technique, which refines the unit cell parameters and profile broadening functions to obtain the best fit between the observed and calculated profiles in the least-squares sense for a given space group. At 350 K, all the observed Bragg peaks could be indexed well with the cubic austenite structure (space group $Fm-3m$) and the refined lattice parameter is found to be $6.00483(4)$ Å. The presence of the superstructure peaks like (111) and (200) in the SXRPD pattern [inset of Fig. 2(a)] confirms that the structure corresponds to the ordered $L2_1$ type [38]. At 235 K, many more reflections appear and the cubic austenite peaks split into two or more peaks clearly indicating a noncubic structure. A careful analysis of all the observed low-intensity peaks revealed that the martensite structure at 235 K cannot be explained in terms of a simple Bain distorted unit cell and requires consideration of modulation of the Bain distorted unit cell as reported in other MSMA [7,8,11,39,40]. Superspace (3+1)D formalism [41–44] is a powerful tool to investigate such complex modulated structures and we employed this formalism to investigate the structure of the modulated martensite phase in $\text{Ni}_2\text{Mn}_{1.4}\text{In}_{0.6}$. Following the superspace group formalism, the SXRPD pattern was divided into two sets of reflections: (1) main reflections corresponding to the Bain distorted basic structure and (2) satellite reflections due to the modulation whose intensity is in general much less than the intensity of the main reflections. All the main reflections corresponding to the basic structure could be indexed with a monoclinic cell with space group $I2/m$ and Le Bail refinement gave us lattice parameters as $a = 4.3983(1)$ Å, $b = 5.6453(2)$ Å, $c = 4.3379(1)$ Å, and $\beta = 92.572(2)^\circ$. After obtaining the cell parameters for the basic structure, the full SXRPD pattern including both the main and the satellite reflections was considered for Le Bail refinement using the superspace group formalism. The satellite reflections were indexed using a modulation wave vector $\mathbf{q} = (0, 0, \frac{1}{3})$ and superspace group $I2/m(\alpha 0 \gamma)00$. Although this commensurate wave vector could index many of the satellite reflections, some of the calculated satellite reflections were found to be shifted away from the observed reflection positions, as can be clearly seen in the inset of Fig. 2(b).

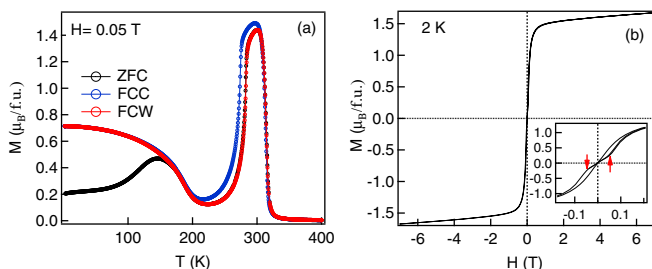


FIG. 1. (a) Magnetization (ZFC, FC, and FW) as a function of temperature at 0.05 T and (b) magnetization as a function of field [$M(H)$] at 2 K. Inset shows the $M(H)$ in expanded scale, where spin-flop transitions are marked by arrows.

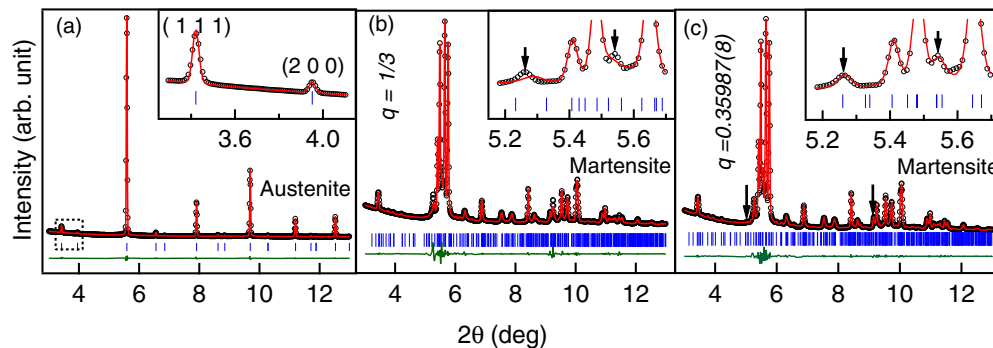


FIG. 2. Le Bail fits for the SXRPD patterns of $\text{Ni}_2\text{Mn}_{1.4}\text{In}_{0.6}$ at (a) cubic austenite phase (350 K). Inset shows superlattice reflections related to $L2_1$ ordering, (b) martensite phase (235 K) with commensurate structure model, and (c) martensite phase (235 K) with incommensurate structure model. The insets show the fit for the main peak region ($2\theta = 5^\circ\text{--}6^\circ$) on an expanded scale. Arrows in (b,c) represent satellite reflections. The experimental data, fitted curve, and the residue are shown by circles (black), continuous line (red), and bottom-most plot (green), respectively. The tick marks (blue) represent the Bragg peak positions.

Therefore the wave vector \mathbf{q} was allowed to be refined and an excellent match between the observed and calculated profiles was obtained for an incommensurate modulation wave vector $\mathbf{q} = 0.35987(8) c^* = (\frac{1}{3} + \delta)c^*$ (where $\delta = 0.02653$ is the degree of incommensuration), including those which could not be accounted for using the commensurate wave vector $\mathbf{q} = \frac{1}{3}$ [see Fig. 2(c)]. This indicates that the martensite phase of $\text{Ni}_2\text{Mn}_{1.4}\text{In}_{0.6}$ has an incommensurate modulation which is $3M$ like (see Ref. [10] for definition of this notation). The SXRPD pattern shows second-order satellites [indicated by blue arrows in Fig. 2(c)] which is consistent with $3M$ -like modulation. A similar $3M$ (sometimes also labeled as $6M$ (for definitions, see Ref. [10]) modulated martensite structure has been reported for another Ni-Mn-In shape-memory alloy composition with martensite transition temperature higher than the present alloy composition [17]. It is interesting to note that the peak broadening of both the main and satellite reflections could be successfully modeled using anisotropic strains as per Stephen's model without invoking fourth-rank strain tensor for phason broadening [45,46]. This is in marked contrast to the situation in Ni_2MnGa where phason strains had to be invoked to model the broadening of the satellite peaks [12].

So far we discussed the results of Le Bail refinements only, where the atomic positions were not refined. Now we proceed to discuss the results of Rietveld refinement, where the atomic positions and atomic modulation functions were also refined. In the Rietveld refinement, Ni, Mn, and In atoms were considered to occupy the $4h$ (0.5 0.25 0), $2a$ (0 0 0), and $2d$ (0 0.5 0) Wyckoff positions, respectively, of the basic structure. The excess Mn atoms occupy the In site ($2d$). Further, the deviation of atoms $u(\bar{x}4)$ from the average structure due to the modulation was modeled using a harmonic atomic modulation function:

$$uj(\bar{x}4) = \sum_{n=1}^{\infty} \{A_n^j \sin[(2\pi n\bar{x}4) + B_n^j \cos(2\pi n\bar{x}4)]\}, \quad (1)$$

where A_n^j and B_n^j are the Fourier amplitudes of the displacement modulation of the j th atom while “ n ” is the order of the Fourier series, which is taken as equivalent to the highest order of the satellite reflections observed [47] which is $n = 2$ in the present case. In the Rietveld refinement, the amplitudes

of the atomic modulation function were refined without any constraints for different atomic sites as per the nonuniform displacement model used in the refinements of the Ni_2MnGa [12] system. While this refinement yields a reasonable fit between the observed and the calculated peak profiles [see Fig. 3(a)], the calculated interatomic distances are physically unrealistic for the Ni-Mn-In family of intermetallic compounds and alloys. For example, the sum of the atomic radii (1.25 Å for Ni, 1.37 Å for Mn, and 1.67 Å for In) of various pairs of atoms is always ≥ 2.5 Å, whereas the interatomic distances obtained after refinement for the nonuniform displacement model are less than 2.3 Å for some t values [see Fig. 4(a)]. One of the reasons for the physically unrealistic interatomic distances could be the presence of antisite disorder commonly observed in Ni-Mn based Heusler alloys. This can in turn affect the amplitude of atomic modulation function, if it is not explicitly accounted for in the refinement. Since Ni and Mn have similar x-ray atomic scattering factors, antisite disorder involving these atoms is not distinguishable by XRD data analysis. On the other hand, the scattering lengths for Ni and Mn for neutrons have opposite signs and hence neutron scattering is ideally suited for capturing Ni-Mn antisite disorder. We therefore performed neutron powder diffraction measurements also. The Rietveld refinement for the austenite

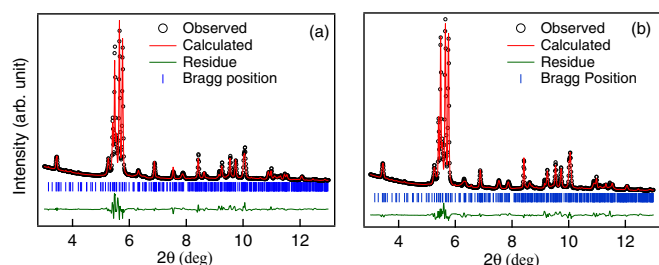


FIG. 3. Rietveld fits for the SXRPD patterns of $\text{Ni}_2\text{Mn}_{1.4}\text{In}_{0.6}$ in martensite phase (235 K) considering (a) a nonuniform atomic displacement (electronic instability model) structure model, and (b) a uniform atomic displacement (adaptive phase) structure model. The experimental data, fitted curve, and the residue are shown by circles (black), continuous line (red), and bottom-most plot (green), respectively. The tick marks (blue) represent the Bragg peak positions.

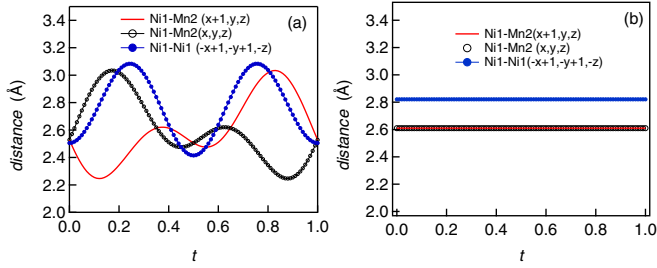


FIG. 4. Distance (selected) as a function of t parameters derived from (a) the Nonuniform atomic displacement model (electronic instability model) showing unphysical values (less than 2.5 Å), and (b) the uniform atomic displacement model (adaptive phase model) showing values that are expected for these kinds of intermetallic compounds and alloys.

phase at room temperature confirmed the absence of any discernible antisite disorder (for details, see the Supplemental Material [24], Sec. A III). In the next step, we therefore considered a “uniform displacement” model for Rietveld refinement in which the amplitudes of modulation for all the atomic sites were constrained to be identical. The results of Rietveld refinement for the uniform displacement model is shown in Fig. 3(b) and the corresponding atomic positions are listed in Table I. The interatomic distances obtained for the refined structure using the uniform atomic displacement model are found to be physically realistic [see Fig. 4(b)] and acceptable for the shape-memory Heusler compounds and alloys. As an additional check, we also carried out refinements for the nonuniform displacement model using constraints on the interatomic distances so that they correspond to physically plausible values. However, these refinements converged to the values obtained for the uniform displacement model. Thus, our results suggest that the modulation in the martensite phase of $\text{Ni}_2\text{Mn}_{1.4}\text{In}_{0.6}$ involves uniform displacement of atoms, which is consistent with the adaptive phase model.

After getting the correct atomic modulation model from the analysis of SXRPD, we now proceed to discuss the magnetic structure of the martensite phase using neutron diffraction data collected at 3 K. Rietveld refinements using neutron diffraction data also support the uniform atomic displacement model (see

TABLE I. Atomic positions (x, y, z), atomic displacement parameter (U_{iso}) and amplitudes (A_1, B_1, A_2, B_2) of the modulation function of the modulated martensite phase (235 K) of $\text{Ni}_2\text{Mn}_{1.4}\text{In}_{0.6}$ obtained from the Rietveld refinement of SXRPD data considering the adaptive phase model.

Wyckoff Modulation		x	y	z	$U_{\text{iso}}(\text{Å}^2)$
Atom position	amplitude				
Ni1	$4h$	0.5	0.25	0	0.0084(5)
Mn1	$2a$	0	0	0	0.0084(5)
In1	$2d$	0	0.5	0	0.0084(5)
Mn2	$2d$	0	0.5	0	0.0084(5)
	A_1	0.1015(7)	0	0.0018(8)	
	B_1	0	0	0	
	A_2	0.0259(14)	0	0.0034(19)	
	B_2	0	0	0	

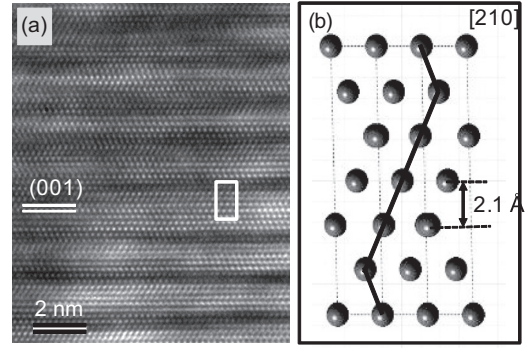


FIG. 5. (a) High-resolution TEM image of the $\text{Ni}_2\text{Mn}_{1.4}\text{In}_{0.6}$ crystal recorded along the [210] zone axis. It represents the martensite phase (100 K). The bright spots correspond to the projected atom rows. The crystal lattice is characterized by a specific stacking of (001) basic planes (distance 2.1 Å), which can be regarded as horizontal twinned lamellae. (b) Crystal lattice model of the unit cell consisting of six (001) planes. The specific stacking, marked by dark lines, corresponds to the uniform displacement model. Since all three kinds of atoms lie in the projection an “average color” is used. The size of such a lattice structure is marked as a rectangle in (a).

the Supplemental Material [24], Sec. A IV for more details). There are four possible magnetic subgroups of the nuclear superspace group $I2/m(\alpha 0 \gamma)00$ (i.e., magnetic superspace groups or mSSGs) due to time reversal symmetry breaking: (i) $I2/m(\alpha 0 \gamma)00$, (ii) $I2'/m(\alpha 0 \gamma)00$, (iii) $I2/m'(\alpha 0 \gamma)00$, and (iv) $I2'/m'(\alpha 0 \gamma)00$. Of these, only (i) and (iv) allow nonzero magnetic moments. The (i) and (iv) mSSGs restrict magnetic moments along the b axis of the monoclinic cell. Out of these two, our Rietveld refinement (see the Supplemental Material [24], Sec. A IV) reveals that the magnetic structure can be described by $I2/m(\alpha 0 \gamma)00$ mSSG in which the magnitude of the Mn magnetic moments of the fully occupied site ($2a$) and partially occupied site ($2d$) are equal ($1.18 \mu_B$) but antiferromagnetically correlated. This is consistent with the double hysteresis-loop-type $M(H)$ plot shown in Fig. 1(b). Thus both the magnetization and neutron results confirm that the low-temperature martensite phase of $\text{Ni}_2\text{Mn}_{1.4}\text{In}_{0.6}$ contains antiferromagnetic correlations.

Additional support for the uniform displacement model was obtained through high-resolution transmission electron microscopy studies (HRTEM). The martensite phase of $\text{Ni}_2\text{Mn}_{1.4}\text{In}_{0.6}$ was observed by *in situ* cooling of the sample down to 100 K. Figure 5(a) shows a noise filtered HRTEM image recorded along the [210] zone. In this crystal lattice projection, atoms appear as bright spots. The (001) atomic planes have an interplanar spacing of 2.1 Å. The occurrence of bright and dark horizontal bands is related to a different stacking of the (001) planes, which generates the unit cell of $3M$ structure. In the martensite phase this is a stacking of six atomic planes ($c = 6 \times 2.15 \text{ Å} = 12.98 \text{ Å}$), which is shown in Fig. 5(b). The corresponding atomic positions are listed in Table S6 of the Supplemental Material [24] for the rational approximant structure of the martensite phase and correlate to the uniform displacement model. In this projection, the twinning of the (001) planes is indicated by a dark zig-zag line within the $3M$ unit cell. The experimental HRTEM image

in (a) includes a region (white rectangle) of such a stacking sequence. The atom positions are consistent with the simulated positions obtained using Rietveld refined coordinates for the uniform displacement model. It has to be mentioned that the *in situ* cooling of the thin TEM samples does not always generate a perfect (4-2) twinned structure of six atomic planes obtained for the average structure using the bulk sample. The HRTEM images often show stacking faults, which locally could lead to different periodicities, say, of seven atomic planes.

The conclusions based on the structure refinements and HRTEM studies were verified using first-principles calculations (the details of which are given in the Supplemental Material [24], Sec. B). Even though we obtained the convergence of the self-consistent calculation for the uniform as well as nonuniform atomic displacement models, many quantities (such as the Fermi energy, local magnetic moments, etc.) appeared to be unrealistic for the nonuniform displacement model. In particular, the total energy appears to be incomparably high (several hundred rydbergs per unit cell) for the nonuniform atomic displacement model with respect to that of the uniform atomic displacement model. Therefore, the nonuniform displacement modulation model does not appear to be realistic.

It is evident from the foregoing results of SXRPD, NPD, and HRTEM investigations as well as the *ab initio* calculations of the ground state that the modulated structure of the $\text{Ni}_2\text{Mn}_{1.4}\text{In}_{0.6}$ Heusler alloy involves uniform displacement of atoms. It is interesting to note that the experimentally observed phonon dispersion curves for Ni_2MnGa reveal a dip in one of the acoustic branches (TA_2) around wave vector $\mathbf{q} \sim (\frac{1}{3} \frac{1}{3} 0)$ whereas the same acoustic branch of $\text{Ni}_2\text{Mn}_{1.4}\text{In}_{0.6}$ ($\sim \text{Ni}_{49.3}\text{Mn}_{34.2}\text{In}_{16.5}$) does not reveal any dip, although the entire branch has rather low energy [19,48–51]. Surprisingly, the previous first-principles calculations for stoichiometric Ni_2MnIn predicted similar qualitative features as those of Ni_2MnGa for the TA_2 phonon branch whereas experimentally Ni_2MnIn does not undergo a martensite transition [19,20,48–51]. This shows that the first-principles calculations are unable to capture the essential features of experimentally observed phonon dispersion curves. However, the difference in the nature of the TA_2 acoustic branch $\text{Ni}_2\text{Mn}_{1.4}\text{In}_{0.6}$ and stoichiometric or off-stoichiometric Ni-Mn-Ga alloys in the experimental phonon dispersion curves clearly suggest that the formation of the martensite phase in the In based alloy may not be mediated

by phonon softening. This provides additional support for the possibility of adaptive modulation in $\text{Ni}_2\text{Mn}_{1.4}\text{In}_{0.6}$ MSMA.

III. CONCLUSIONS

To summarize, we have critically evaluated the applicability of two existing models (electronic instability and the nanotwinning based adaptivity models) for the origin of modulation in the $\text{Ni}_2\text{Mn}_{1.4}\text{In}_{0.6}$ magnetic shape-memory alloy. We carried out Rietveld analysis of high-resolution SXRPD and powder neutron diffraction patterns of the austenite and modulated martensite phases of $\text{Ni}_2\text{Mn}_{1.4}\text{In}_{0.6}$ using (3+1)D superspace formalism. We have considered both nonuniform and uniform displacement models of incommensurate modulation in the Rietveld refinements and shown that the nature of modulation in $\text{Ni}_2\text{Mn}_{1.4}\text{In}_{0.6}$ involves uniform atomic displacement of atoms as expected for the model based on adaptivity. This is also supported by HRTEM and *ab initio* calculations. However, investigation of electronic structure using single crystal of $\text{Ni}_2\text{Mn}_{1.4}\text{In}_{0.6}$ MSMA will be of further use for unambiguous proof of adaptivity in this system. Further we have shown that the magnetic structure of the martensite phase at 3K is site disordered antiferromagnetic where Mn atoms at two different crystallographic positions are coupled antiferromagnetically. The present study underlines the importance of superspace group analysis of the diffraction data to understand the physics of modulation in magnetic shape-memory Heusler alloys.

ACKNOWLEDGMENTS

We thank Branton Campbell for useful discussion. S.S. thanks the Alexander von Humboldt foundation, Germany, for support through the Research Fellowship, and the Science and Engineering Research Board of India for support through the award of the Ramanujan Fellowship. The support from DST under its India-DESY scheme through Jawaharlal Nehru Centre for Advanced Scientific Research is acknowledged. B.D. acknowledges Deutsche Forschungsgemeinschaft (Germany) for the financial support within the priority Program No. SPP1599. D.P. thanks the Science and Engineering Research Board of India for the support through the award of the J. C. Bose National Fellowship. V.P. acknowledges the support of Project No. LO1603 under the Ministry of Education, Youth and Sports National Sustainability Program I of the Czech Republic.

-
- [1] K. Ullakko, J. K. Huang, C. Kantner, R. C. O’Handley, and V. V. Kokorin, *Appl. Phys. Lett.* **69**, 1966 (1996).
 - [2] T. Krenke, E. Duman, M. Acet, E. F. Wassermann, X. Moya, L. Manosa, and A. Planes, *Nat. Mater.* **4**, 450 (2005).
 - [3] L. Manosa, D. Gonzalez-Alonso, A. Planes, E. Bonnot, M. Barrio, J.-L. Tamarit, S. Aksoy, and M. Acet, *Nat. Mater.* **9**, 478 (2010).
 - [4] I. Dubenko, A. K. Pathak, S. Stadler, N. Ali, Y. Kovarskii, V. N. Prudnikov, N. S. Perov, and A. B. Granovsky, *Phys. Rev. B* **80**, 092408 (2009).
 - [5] B. M. Wang, Y. Liu, P. Ren, B. Xia, K. B. Ruan, J. B. Yi, J. Ding, X. G. Li, and L. Wang, *Phys. Rev. Lett.* **106**, 077203 (2011).
 - [6] S. Singh, L. Caron, S. W. D’Souza, T. Fichtner, G. Porcari, S. Fabbri, C. Shekhar, S. Chadov, M. Solzi, and C. Felser, *Adv. Mater.* **28**, 3321 (2016).
 - [7] L. Righi, F. Albertini, G. Calestani, L. Pareti, A. Paoluzi, C. Ritter, P. A. Algarabel, L. Morellon, and M. Ricardo Ibarra, *J. Solid State Chem.* **179**, 3525 (2006).
 - [8] P. J. Brown, J. Crangle, T. Kanomata, M. Matsumoto, K. U. Neumann, B. Ouladdiaf, and K. R. A. Ziebeck, *J. Phys.: Condens. Matter* **14**, 10159 (2002).

- [9] S. Sanjay, J. Nayak, R. Abhishek, R. Parasmani, H. H. Adrian, S. R. Barman, and P. Dhananjai, *J. Phys.: Condens. Matter* **25**, 212203 (2013).
- [10] S. Singh, S. R. Barman, and D. Pandey, *Z. Kristallogr.* **230**, 13 (2015).
- [11] S. Singh, J. Bednarcik, S. R. Barman, C. Felser, and D. Pandey, *Phys. Rev. B* **92**, 054112 (2015).
- [12] S. Singh, V. Petricek, P. Rajput, A. H. Hill, E. Suard, S. R. Barman, and D. Pandey, *Phys. Rev. B* **90**, 014109 (2014).
- [13] S. W. D'Souza, A. Rai, J. Nayak, M. Maniraj, R. S. Dhaka, S. R. Barman, D. L. Schlagel, T. A. Lograsso, and A. Chakrabarti, *Phys. Rev. B* **85**, 085123 (2012).
- [14] M. E. Gruner, S. Fähler, and P. Entel, *Phys. Status Solidi* **251**, 2067 (2014).
- [15] S. Kaufmann, U. K. Rößler, O. Heczko, M. Wuttig, J. Buschbeck, L. Schultz, and S. Fähler, *Phys. Rev. Lett.* **104**, 145702 (2010).
- [16] R. Niemann, U. K. Rößler, M. E. Gruner, O. Heczko, L. Schultz, and S. Fähler, *Adv. Eng. Mater.* **14**, 562 (2012).
- [17] H. Yan, Y. Zhang, N. Xu, A. Senyshyn, H.-G. Brokmeier, C. Esling, X. Zhao, and L. Zuo, *Acta Mater.* **88**, 375 (2015).
- [18] A. Zheludev, S. M. Shapiro, P. Wochner, A. Schwartz, M. Wall, and L. E. Tanner, *Phys. Rev. B* **51**, 11310 (1995).
- [19] A. Zheludev, S. M. Shapiro, P. Wochner, and L. E. Tanner, *Phys. Rev. B* **54**, 15045 (1996).
- [20] U. Stuhr, P. Vorderwisch, V. V. Kokorin, and P. A. Lindgård, *Phys. Rev. B* **56**, 14360 (1997).
- [21] A. Pramanick, X. P. Wang, K. An, A. D. Stoica, J. Yi, Z. Gai, C. Hoffmann, and X. L. Wang, *Phys. Rev. B* **85**, 144412 (2012).
- [22] S. Banik, S. Singh, R. Rawat, P. K. Mukhopadhyay, B. L. Ahuja, A. M. Awasthi, S. R. Barman, and E. V. Sampathkumaran, *Br. J. Appl. Phys.* **106**, 103919 (2009).
- [23] S. M. Shapiro, P. Vorderwisch, K. Habicht, K. Hradil, and H. Schneider, *EPL* **77**, 56004 (2007).
- [24] See Supplemental Material at <http://link.aps.org/supplemental/10.1103/PhysRevB.97.224102> for experimental details and results on sample preparation, measurements [magnetization, SXRPD, NPD, and high-resolution transmission electron microscopy (HRTEM)], Rietveld refinements, and first-principles calculations. Also see Refs. [25–36].
- [25] S. Singh, P. Kushwaha, F. Scheibel, H.-P. Liermann, S. R. Barman, M. Acet, C. Felser, and D. Pandey, *Phys. Rev. B* **92**, 020105 (2015).
- [26] V. Petricek, M. Dušek, and L. Palatinus, *Z. Kristallogr.* **229**, 345 (2014).
- [27] R. Kilaas, *J. Microsc.* **190**, 45 (1998).
- [28] K. Momma and F. Izumi, *J. Appl. Cryst.* **44**, 1272 (2011).
- [29] P. Stadelmann, Jems, <http://cimewww.epfl.ch/people/stadelmann/jemswebsite/jems.html>
- [30] H. Ebert, D. Ködderitzsch, and J. Minár, *Rep. Prog. Phys.* **74**, 096501 (2011).
- [31] S. H. Vosko, L. Wilk, and M. Nusair, *Can. J. Phys.* **58**, 1200 (1980).
- [32] G. Kresse and J. Hafner, *Phys. Rev. B* **47**, 558 (1993).
- [33] G. Kresse and J. Furthmüller, *Phys. Rev. B* **54**, 11169 (1996).
- [34] P. E. Blöchl, *Phys. Rev. B* **50**, 17953 (1994).
- [35] J. P. Perdew, K. Burke, and M. Ernzerhof, *Phys. Rev. Lett.* **77**, 3865 (1996).
- [36] H. J. Monkhorst and J. D. Pack, *Phys. Rev. B* **13**, 5188 (1976).
- [37] S. Aksoy, M. Acet, P. P. Deen, L. Mañosa, and A. Planes, *Phys. Rev. B* **79**, 212401 (2009).
- [38] S. R. Barman, A. Chakrabarti, S. Singh, S. Banik, S. Bhardwaj, P. L. Paulose, B. A. Chalke, A. K. Panda, A. Mitra, and A. M. Awasthi, *Phys. Rev. B* **78**, 134406 (2008).
- [39] S. Singh, K. R. A. Ziebeck, E. Suard, P. Rajput, S. Bhardwaj, A. M. Awasthi, and S. R. Barman, *Appl. Phys. Lett.* **101**, 171904 (2012).
- [40] S. Singh, R. Rawat, and S. R. Barman, *Appl. Phys. Lett.* **99**, 021902 (2011).
- [41] P. De Wolff, *Acta Crystallogr., Sect. A: Cryst. Phys., Diffraction, Theor. Gen. Crystallogr.* **30**, 777 (1974).
- [42] P. De Wolff, *Acta Crystallogr., Sect. A: Cryst. Phys., Diffraction, Theor. Gen. Crystallogr.* **33**, 493 (1977).
- [43] M. Dusek, V. Petricek, M. Wunschel, R. E. Dinnebier, and S. van Smaalen, *J. Appl. Crystallogr.* **34**, 398 (2001).
- [44] T. Janssen, A. Janner, A. Looijenga-Vos, and P. De Wolff, in *International Tables for Crystallography, Vol. C: Mathematical, Physical and Chemical Tables*, edited by E. Prince (Wiley, New York, 2004), Chap. 9.8, p. 907.
- [45] A. Leineweber and V. Petricek, *J. Appl. Crystallogr.* **40**, 1027 (2007).
- [46] P. Stephens, *J. Appl. Crystallogr.* **32**, 281 (1999).
- [47] S. Van Smaalen, *Incommensurate Crystallography* (Oxford University Press, New York, 2007).
- [48] X. Moya, D. González-Alonso, L. Mañosa, A. Planes, V. O. Garlea, T. A. Lograsso, D. L. Schlagel, J. L. Zarestky, S. Aksoy, and M. Acet, *Phys. Rev. B* **79**, 214118 (2009).
- [49] M. Acet, L. Manosa, and A. Planes, *Handbook of Magnetic Materials* (Elsevier, Amsterdam, 2011), Vol. 19, Chap. 4.
- [50] C. Bungaro, K. M. Rabe, and A. Dal Corso, *Phys. Rev. B* **68**, 134104 (2003).
- [51] A. T. Zayak, P. Entel, K. M. Rabe, W. A. Adeagbo, and M. Acet, *Phys. Rev. B* **72**, 054113 (2005).